

# Ionization state and geometry of the extragalactic HII region SMC-N88A for the interpretation of observations of galaxies in the epoch of reionization

C.G. Díaz<sup>1</sup>, D. Mast<sup>2</sup>, G. Oio<sup>3</sup> & R. Bassett<sup>4</sup>

<sup>1</sup> *Instituto de Ciencias Astronómicas, de la Tierra y del Espacio, CONICET-UNSJ, Argentina*

<sup>2</sup> *Observatorio Astronómico de Córdoba, UNC, Argentina*

<sup>3</sup> *Chinese Academy of Sciences South America Center for Astronomy (CASSACA), China*

<sup>4</sup> *Swinburne University of Technology, Australia*

Contact / gonzalodiaz@conicet.gov.ar

**Resumen** / Los fotones ionizantes de las primeras galaxias contribuyeron a la progresiva re-ionización del hidrógeno intergaláctico, que terminó a  $z \sim 6$ . Una de las principales incógnitas de este proceso es la fracción de fotones ionizantes que escapan de las galaxias y alcanzan el medio intergaláctico durante esta época. Sin embargo, ningún telescopio puede detectar directamente esta radiación en objetos a  $z \geq 6$  porque es absorbida por el hidrógeno neutro del medio intergaláctico en el mismo proceso de reionización cósmica. Por este motivo se han propuesto varios indicadores alternativos del escape de fotones ionizantes, basados tanto en líneas de emisión como de absorción. En este trabajo, el objetivo a largo plazo es poner a prueba los modelos utilizados en la interpretación de las observaciones de líneas de emisión nebulares de galaxias a muy alto redshift. Hemos observado dos regiones H II compactas de la Nube Menor de Magallanes con la unidad de campo integrado (o IFU) de GMOS-S, para estudiar la física involucrada en el escape de fotones ionizantes producidos por estrellas masivas que habitan en regiones H II jóvenes. A una distancia de  $\sim 61$  kpc, la cercanía de estos objetos hace posible estudiar la geometría y cinemática del gas en emisión con una resolución espacial inalcanzable en galaxias de la época de reionización. En esta oportunidad, presentamos las bases del proyecto y el estado de los datos obtenidos para SMC-N88A.

**Abstract** / Ionizing photons from the first galaxies contributed to the progressive re-ionization of the intergalactic hydrogen, which ended by  $z \sim 6$ . One of the main unknowns of this process is the fraction of ionizing photons that escape from galaxies and reach the intergalactic medium during this epoch. However, no telescope can directly detect this radiation on objects at  $z \geq 6$  because it is absorbed by the neutral hydrogen of the intergalactic medium in the same cosmic reionization process. For this reason, several alternative indicators of the escape of ionizing photons have been proposed, based on both emission and absorption lines. In this work, the long-term goal is to test the models used in the interpretation of observations of nebular emission lines from galaxies at very high redshift. We have observed two compact H II regions of the Small Magellanic Cloud with the Integral Field Unit (or IFU) of GMOS-S, to study the physics involved in the escape of ionizing photons produced by massive stars inhabiting young H II regions. At a distance of  $\sim 61$  kpc, the proximity of these objects makes it possible to study the geometry and kinematics of the gas in emission with a spatial resolution unattainable in galaxies of the reionization epoch. In this opportunity, we present the bases of the project and the data obtained for SMC-N88A.

**Keywords** / galaxies: high-redshift — intergalactic medium — galaxies: ISM — HII regions

## 1. Introduction

The contribution of galaxies to the reionization of intergalactic hydrogen at redshift  $z > 6$  depends on the fraction of ionizing photons that reach the intergalactic medium (IGM) after being produced by young massive stars. This quantity is usually expressed in terms of the escape fraction ( $f_{\text{esc}}^{\text{LyC}}$ ) of photons in the hydrogen Lyman series continuum (LyC,  $\lambda < 912 \text{ \AA}$ ). However, LyC radiation is not observable in objects at  $z > 6$  because it is absorbed by the neutral hydrogen of the IGM in the same cosmic reionization process. For this reason, an alternative  $f_{\text{esc}}^{\text{LyC}}$  indicator is essential to study this phenomenon directly at the Epoch of Reionization (EoR), thus  $f_{\text{esc}}^{\text{LyC}}$  indicators have been proposed throughout the spectral range, including: Ly $\alpha$  emission (Verhamme

et al., 2015), H I absorption lines (Lyman series) and low ionization metals like [Si II]( $\lambda 1190, \lambda 1260$ ) (Chisholm et al., 2018), Mg II( $\lambda \lambda 2796, 2803$ ) emission (Henry et al., 2018), nebular emission lines ratios of the visible spectrum such as O32 ([O III]( $\lambda 5007$ )/[O II]( $\lambda \lambda 3727, 3729$ )) (Izotov et al., 2018), deficiency in [S II]( $\lambda \lambda 6717, 6731$ ) (Wang et al., 2021), infrared emission lines in the range  $5 \mu\text{m}$  to  $120 \mu\text{m}$  (Ramambason et al., 2022), and the list is growing.

The direction of LyC photon escape is conditioned by the distribution of gas and dust in the source (e.g. Kostyuk et al., 2022), with most ionizing photons escaping from low density channels (Yeh et al., 2023). Thus,  $f_{\text{esc}}^{\text{LyC}}$  depends on the line of sight and the conditions of individual H II regions hosting massive bright stars. However, spectroscopic observations of a distant galaxy

correspond to scales of kiloparsecs (e.g.:  $\sim 7.8$  kpc/'' at  $z = 3$  and  $\sim 5.8$  kpc/'' at  $z = 6$ , assuming a  $\lambda$ CDM cosmology with  $H_0 = 70 \text{ km s}^{-1} \text{ Mpc}^{-1}$ ), thus integrating the light of many, if not all, H II regions of the observed galaxy, in a single measurement.

In this contribution, we report the start of a project to study the internal structures of two individual H II regions with high spatial resolution, using Integral Field Spectroscopic observations over a wide spectral range. Since it is not possible to resolve individual H II regions in galaxies during the EoR, we turned to the closest local analogue: the Small Magellanic Cloud (SMC). The long-term goal is to improve our interpretation of the observed nebular emission line ratios in EoR galaxies and their relationship to LyC photon escape. In particular, the primary objectives are: 1- to determine the effect of geometry and gas structure on the escape of ionizing photons from individual H II regions, and 2- to test the relative stability of the indicator S32 ( $[\text{S III}]\lambda 9069 + \lambda 9531 / [\text{S II}](\lambda \lambda 6717, 6731)$ ) with respect to O32, as predicted by models used in the interpretation of galaxy observations.

## 2. Sample

The Magellanic Clouds are satellites of the Milky Way in the mass range of the EoR galaxies. In particular, the stellar mass of the SMC ( $M_* \sim 5.3 \times 10^8 M_\odot$ , Rubele et al., 2018) is in the range predicted by current models for the main contributors of LyC during the EoR at  $z \sim 7$  (Yeh et al., 2023). Also, the radius of  $\sim 3$  kpc (Stanimirović et al., 2004) and a low metallicity of  $[\text{Fe}/\text{H}] \sim -1$  dex (e.g. Choudhury et al., 2020; De Bortoli et al., 2022)) are common features of EoR galaxies. Moreover, the proximity of the SMC grants a spatial resolution unattainable in galaxies during the EoR. As a result, the SMC is a good laboratory to test the escape of ionizing photons produced by massive stars during the EoR.

The sample includes two compact H II regions in the SMC, selected for their brightness and size, and a low number of known hosted stars. SMC N88A (R.A. = 01 h 24 m 8.3 s, Dec. =  $-73^\circ 09' 04''$ ,  $V = 12.18$  mag) is located in the SMC at a distance  $d \sim 62.4$  kpc (Graczyk et al., 2020), has an angular size  $\sim 5$  arcsec that corresponds to 1.5 pc in diameter, and its dominant star is type O6. The second target is SMC N81 (R.A. = 01 h 09 m 12.94 s, Dec. =  $-73^\circ 11' 39''$ ,  $V = 11.7$  mag), which is not included in this report.

## 3. Observations

The relative stability of S32 with respect to O32 must be evaluated in a robust way, for which it is necessary to observe both line ratios in the same object and with the same instrument. Currently, the Gemini Multi-Object Spectrograph (GMOS, Hook et al., 2004), at the Gemini South and Gemini North telescopes are the only instruments in the world that meet the three conditions necessary for this work, which are: *i*) to cover the spectral range from  $[\text{O II}](\lambda \lambda 3727, 3729)$  to  $[\text{S III}](\lambda 9531)$ , *ii*)

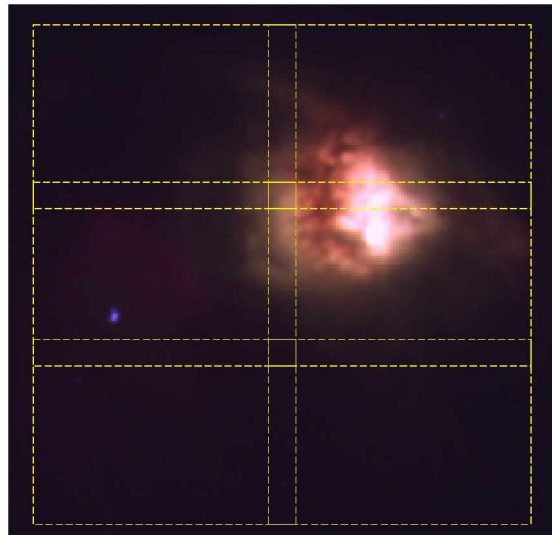


Figure 1: False-color image composition of SMC N88A using data from the Wide Field Camera (Hubble Space Telescope). Red is F656n (H $\alpha$ ), green is F502n ([O III]), and blue is F487n (H $\beta$ ). Each yellow dashed rectangle represents a field of GMOS IFU-R ( $5.0 \times 3.5$  arcsec $^2$ ). The mosaic is composed of 6 fields covering a  $9.5 \times 9.5$  arcsec $^2$  area.

to observe both factors of an emission line ratio (e.g. [O II] and [O III]) with the same configuration, and *iii*) to provide spatially resolved spectroscopy.

The data for the project were obtained with the Integral Field Unit (IFU) of GMOS-S (Allington-Smith et al., 2002; Gimeno et al., 2016). SMC N88A was observed with six pointings of  $3.5 \times 5$  arcsec (i.e. the field of view of IFU-R), on a rectangular pattern of 3 by 2 with a 0.5 arcsec overlap between adjacent frames (Fig. 1). The coverage of GMOS observations of SMC-N88A demonstrates the capability of resolving structures within the H II region.

Two configurations were used with the IFU-R mask. The “blue” configuration, which included the unfiltered B600 grating with a central wavelength  $\lambda_c = 500$  nm to cover [O II] and [O III] simultaneously; and the “red” configuration, which included the R400 grating with the OG515 filter and central wavelength  $\lambda_c = 890$  nm to cover [S II] and [S III] simultaneously. The spectral resolution obtained is  $1.94 \text{ \AA}$  ( $\sim 115 \text{ km s}^{-1}$  at  $5007 \text{ \AA}$ ) in the blue, and  $2.87 \text{ \AA}$  ( $\sim 95 \text{ km s}^{-1}$  at  $9000 \text{ \AA}$ ) in the red, sampled to 3.8 pixels, which is sufficient to test the S32 and O32 diagnostics, and to compare with models and observations of galaxies. Three exposures of 60s were acquired at each pointing for the blue and red configuration, making a total of 36 science data cubes. Additionally, a telluric comparison star was observed in the red configuration prior the science observations. This was used to remove the atmospheric absorption at  $9500 \text{ \AA} - 9600 \text{ \AA}$  that severely affects the [S III] sulfur line ( $\lambda 9531$ ). The data were acquired for program GS-2019B-Q-205\* on October 10th (red configuration)

\*PI: R. Bassett. The data are publicly available from the Gemini Observatory Archive at <https://archive.gemini.edu/searchform>

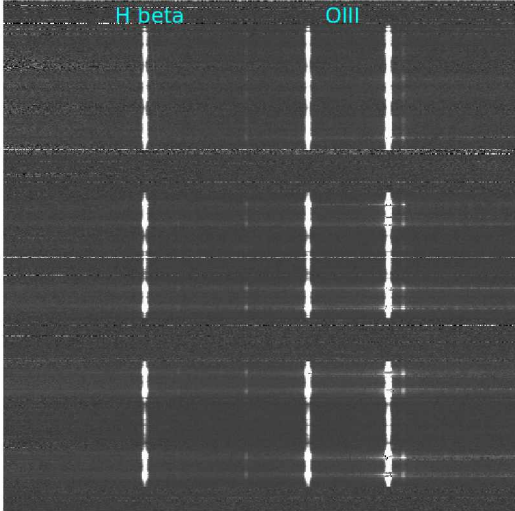


Figure 2: Small region from a sky-subtracted 2D spectrum of a single exposure with the blue configuration, centred on the emission from  $H\beta$  and  $[OIII]$ . Wavelength increases to the right. Each row contains the spectrum from a different fiber. The horizontal areas where the emission lines are not visible correspond to sky fibers.

and November 28th (blue configuration), 2019. The flux standard star C32 was observed with both configurations on July 24th, 2019. Conditions during observations were photometric (clear of clouds) and the image quality (the FWHM of a point source) was  $< 0.85$  arcsec in the  $g'$ -band, implying a spatial resolution  $< 0.25$  pc for SMC N88A.

The data reduction process included the following calibration observations: 15 BIAS, seven FLATS, seven ARCS, three telluric star exposures, and two flux standard star exposures. All of these are currently being processed with the GEMINI IRAF package, provided by the Gemini Observatory. Following the basic instructions, the processing requires BIAS combination and subtraction, removal of the overscan region, creation of a bad pixel mask (BPM) for each individual exposure (including FLAT images), adding the BPM to the data quality (DQ) extension of each science exposure, creation of an image for tracing the position of individual spectra from the FLAT, FLAT field normalization, removal of CCD gaps, wavelength calibration, quantum efficiency correction, sky subtraction, datacube reconstruction, telluric correction, and mosaic building. Fig. 2 shows a small region of the 2D spectrum of a single exposure from the middle row second column pointing of Fig. 1, in the blue configuration. Data reduction is currently at the datacube reconstruction step.

#### 4. Methodology

First, the stability of S32 and O32 as indicators of  $f_{\text{esc}}^{\text{LyC}}$  is tested as follows. The flux of  $[OII]$ ,  $[OIII]$ ,  $[SIII]$  and  $[SII]$  is measured in each spaxel of the cube to obtain the distribution of O32 and S32 values across the region. The total emission flux of each line is obtained by integration over all spaxels to calculate the integrated S32

and O32 ratios similar to high redshift galaxies. Then, we will determine the discrepancies between the integrated values and the distribution functions, based on statistical tests of the mean, the dispersion, and the range of values.

Second, we will exploit the spatial coverage of the data. Maps of S32 and O32 will be obtained and the spatial correlation will be determined using image overlapping and cross-matching tools. The values with the highest and least correlation will be identified, and their locations within the  $HII$  region will be compared to known structures like dust lines, shells, winds, etc. We will also determine the location of the maximum and minimum values of S32 and O32, and the radial profiles. The slope of the profiles will be compared with the level of spatial correlation between the two indicators, as well as known structures in the region.

Third, we will calculate the LyC radiation that escapes from the region as  $F_{\text{out}} = F_{\text{in}} - F_{\text{em}}$  and  $f_{\text{esc}}^{\text{LyC}} = F_{\text{out}}/F_{\text{in}}$ . The intrinsic LyC flux ( $F_{\text{in}}$ ) emitted by the ionizing sources is obtained from fitting BPASS stellar templates (Eldridge et al., 2017) to the spectra of the central stars. The ionizing flux re-emitted by the nebula ( $F_{\text{em}}$ ) is determined by the total flux in hydrogen emission lines, aided by photo-ionization models from MOCASSIN3D (Ercolano et al., 2003). This measurements will be a strong test to prediction of  $f_{\text{esc}}^{\text{LyC}}$  from integrated O32 and S32 ratios, typically used in high redshift galaxies observations.

#### 5. Summary

This work is based on IFU observations of the compact  $HII$  region SMC-N88A, to study the spatial correlation between the ratios O32 and S32, the areas of high  $f_{\text{esc}}^{\text{LyC}}$ , and other known structures. It proposes a test for the effect of geometry and orientation in the inference of  $f_{\text{esc}}^{\text{LyC}}$  in high redshift galaxies.

#### References

- Allington-Smith J., et al., 2002, PASP, 114, 892
- Chisholm J., et al., 2018, A&A, 616, A30
- Choudhury S., et al., 2020, MNRAS, 497, 3746
- De Bortoli B.J., et al., 2022, A&A, 664, A168
- Eldridge J.J., et al., 2017, PASA, 34, e058
- Ercolano B., et al., 2003, MNRAS, 340, 1136
- Gimeno G., et al., 2016, *Society of Photo-Optical Instrumentation Engineers (SPIE) Conference Series*, vol. 9908, 99082S
- Graczyk D., et al., 2020, ApJ, 904, 13
- Henry A., et al., 2018, ApJ, 855, 96
- Hook I.M., et al., 2004, PASP, 116, 425
- Izotov Y.I., et al., 2018, MNRAS, 478, 4851
- Kostyuk I., et al., 2022, arXiv e-prints, arXiv:2207.11278
- Ramambason L., et al., 2022, A&A, 667, A35
- Rubele S., et al., 2018, MNRAS, 478, 5017
- Stanimirović S., Staveley-Smith L., Jones P.A., 2004, ApJ, 604, 176
- Verhamme A., et al., 2015, A&A, 578, A7
- Wang B., et al., 2021, ApJ, 916, 3
- Yeh J.Y.C., et al., 2023, MNRAS